Available online at www.sciencedirect.com
SCIENCE DIRECT®
Comput. Methods Appl. Mech. Engrg. 193 (2004) 679–699
Computer methods in applied mechanics and engineering
www.elsevier.com/locate/cma

Modeling and simulation of a class of coupled thermo-chemo-mechanical processes in multiphase solids

T.I. Zohdi *

Department of Mechanical Engineering, University of California, 6195 Etcheverry Hall, Berkeley, CA 94720-1740, USA

Received 3 September 2003; received in revised form 30 October 2003; accepted 1 November 2003

Abstract

In this work a model and solution strategy are developed to describe a class of coupled thermo-chemo-mechanical systems involving the solid-state diffusion of a dilute solute into a multiphase solid material, the subsequent reactions, production of heat, changes in the stress fields, and the evolution of material degradation and inelastic strains in the solid. The algorithm involves recursive staggering, whose convergence is dependent on the discretized time step size. Because the multifield coupling can change, becoming stronger, weaker, or possibly oscillatory, it is extremely difficult to ascertain a-priori the time step size needed to meet a prespecified tolerance on the staggering error, i.e. the incomplete resolution of the interaction between the fields. The solution process involves time step size adaptivity to control the contraction mapping constant of the multifield system operator in order to induce desired staggering rates of convergence within each time step, and hence, the staggering error. Three-dimensional numerical experiments are performed to illustrate the behavior of the model and the solution strategy.

Keywords: Thermo-chemo-mechanical coupling; Multiphase materials

1. Introduction

In many applications, multifield models arise from a description of thermo-chemical reactions occurring in deformable multiphase solids (Fig. 1). Relevant examples include certain problems of environmental mechanics concerned with the detrimental chemical attack on solids by volatile gases or liquid solutes which come in contact with structural surfaces and then diffuse into the subsurface. The subsequent reactions lead to loss of structural integrity. In this work aspects of the modeling and numerical simulation of such strongly coupled thermo-chemical processes in multiphase solids are discussed. A general multifield model is developed which describes the diffusion of a dilute solute into a heterogeneous solid material, its subsequent reactions, production of heat, changes in the stress fields and the evolution of material changes and inelastic strains within the solid. The modeling and solution algorithms are general enough to be applicable

* Tel.: +1-510-642-6834; fax: +1-510-642-6163.
E-mail address: zohdi@newton.berkeley.edu (T.I. Zohdi).

0045-7825/$ - see front matter
doi:10.1016/j.cma.2003.11.006

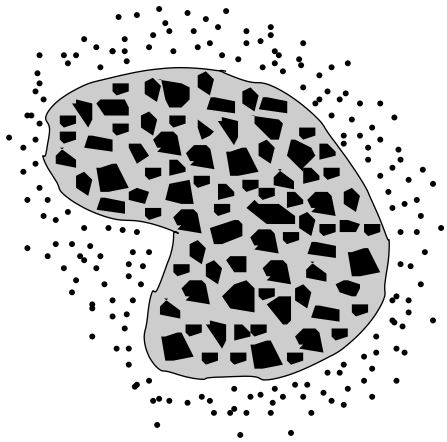

Fig. 1. Diffusion of a small species into a heterogeneous medium.

to a wide range of long-term thermo-chemo-mechanical phenomena associated with damage in materials with heterogeneous microstructure. For experimental and theoretical overviews, we refer the reader to the series of works by Huet and coworkers [17–24]. For general overviews in the area of heterogeneous materials see Nemat-Nasser and Hori [41]. Although the emphasis will be on the simulation of long-term multifield phenomena, the analysis in this work is also applicable to shorter time-scale problems involving thermo-chemical processing such as self-propagating high-temperature synthesis (SHS), whereby chemical reactions are initiated on the surface of a material to be processed. In the method, the substantial heat evolved by surface chemical reactions sustain and propagate thermo-chemical processes. This approach is a relatively new economical way of manufacturing advanced materials. For example by initiating a highly exothermic surface thermal reaction between bonded titanium powder in a nitrogen gas atmosphere, an initial amount of titanium-nitride, $\mathrm{Ti}(s) + 1/2\mathrm{N}_2(g) = \mathrm{TiN}(s)$, which a desirable product, is produced. This process releases substantial heat, which produces a combustion front which propagates throughout the solid. A wide variety of materials, ceramics, intermetallic compounds and composites can be produced by SHS. For an introduction see the texts of Ashby and Jones [5] or Shackleford [52]. Generally speaking, such processes are related to controlled combustion methods [50], whereby a chemical species acts as a catalyst to promote reactions, for example in chemical separation and polymerization. A related processing method is Shock Induced Chemical Reactions (SICR), whereby a shock wave is passed through chemical reacting powders, which sinters them together. Some relevant work in the modeling and simulation of such processes can be found in Thadhani [55], Nesterenko et al. [43], Vecchio and Meyers [56] and Meyers et al. [36]. For a review of such methods see Meyers [37] or Nesterenko [42].

2. A model problem involving multifield processes in multiphase solids

A structure which occupies an open bounded domain in $\Omega \in \mathbb{R}^3$, with boundary $\partial\Omega$, is considered. The boundary consists of (1) Γ_c and Γ_g, where the solute concentrations (c) and solute fluxes are respectively specified, (2) Γ_u on which the displacements ($\boldsymbol{u}$) are prescribed and a part Γ_t on which tractions are prescribed, and (3) Γ_θ on which the temperature (θ) is prescribed, and a part Γ_q on which thermal fluxes are prescribed. The primary (familiar) mechanical, thermal, and diffusive properties of the heterogeneous material are characterized by a spatially varying elasticity tensor $\mathbb{E} \in \mathbb{R}^{3^2\times 3^2}$, a spatially varying conductivity tensor $\mathbb{K} \in \mathbb{R}^{3\times 3}$, and a spatially varying diffusivity tensor $\mathbb{D}_0 \in \mathbb{R}^{3\times 3}$ (at a reference temperature), all

of which are assumed to be symmetric bounded positive definite tensor-valued functions. Other material properties will be introduced during the development of the overall model. For reasons of clarity, strong forms are used to derive the governing equations, possibly assuming more regularity than warranted. Afterwards, only the weak forms, which produce solutions which coincide with strong forms when the solutions are smooth enough, are employed. The use of weak forms are important for this class of problems due to the heterogeneous microstructure, which leads to particularly rough solution fields.

3. Constitutive assumptions

We consider the case of moderate finite deformations involving elastic and inelastic strains. Later in the work, an updated Lagrangian staggering type scheme, formulated directly in the (deformed) current configuration, will be developed, and thus Eulerian-based material laws are advantageous. A relatively straightforward extension to classical *isotropic* infinitesimal deformation constitutive models is to employ the Eulerian (or Almansi) strain tensor [1]

$$\boldsymbol{\sigma} = \alpha \mathbb{E}_0 : (\boldsymbol{e} - \boldsymbol{\beta}), \tag{3.1}$$

where $\boldsymbol{\sigma}$ is the Cauchy stress, where $\boldsymbol{e} = \frac{1}{2}(\nabla_x \boldsymbol{u} + (\nabla_x \boldsymbol{u})^{\mathrm{T}} - (\nabla_x \boldsymbol{u})^{\mathrm{T}} \cdot \nabla_x \boldsymbol{u})$, where $\boldsymbol{\beta} = \boldsymbol{e}_\theta + \boldsymbol{e}_\lambda + \boldsymbol{e}_\varphi$, where $\boldsymbol{e}_\theta \overset{\text{def}}{=} \boldsymbol{\gamma} \cdot (\theta - \theta_0)\mathbf{1}$, where $\boldsymbol{e}_\lambda$ represents deviatoric-like inelastic strains, for example plastic-like strains, where $\boldsymbol{e}_\varphi$ represents dilatational-like inelastic strains, for example representing gas that occurs as a reaction byproduct, and where $\boldsymbol{e}_\theta$ represents thermal strains. Here, the current value of the elasticity tensor is $\mathbb{E} = \alpha \mathbb{E}_0$, where $\mathbb{E}_0$ represents the virgin isotropic undamaged material, where $0 \leqslant \alpha \leqslant 1$ is the scalar continuity (isotropic damage) parameter [31], where $\alpha(t = 0) = 1$ indicates the initial undamaged state and where $\alpha \to 0$ indicates a completely damaged state. The introduced quantities are modeled as being governed by evolution over-stress functions of the form

$$\begin{aligned}
&\dot{\alpha} = \underbrace{\left(a_1 c + a_2 \left(\frac{\|\boldsymbol{\sigma}'\|}{\|\boldsymbol{\sigma}'_{\text{crit}}\|} - 1 \right) + a_3 \left(\frac{|\operatorname{tr} \boldsymbol{\sigma}|}{|\operatorname{tr} \boldsymbol{\sigma}_{\text{crit}}|} - 1 \right) \right)}_{g_\alpha} \alpha \quad (0 < \alpha \leqslant 1), \\
&\dot{\lambda} = \underbrace{\left(a_4 \left(\frac{\|\boldsymbol{S}'\|}{\|\boldsymbol{S}'_{\text{crit}}\|} - 1 \right) \right)}_{g_\lambda} \lambda \Rightarrow \boldsymbol{e}_\lambda \overset{\text{def}}{=} \boldsymbol{F} \cdot \left(\int_0^t \dot{\lambda} \boldsymbol{h} \, \mathrm{d}t \right) \cdot \boldsymbol{F}^{\mathrm{T}} \left(\boldsymbol{h} = {}^{\text{def}} \frac{\boldsymbol{S}'}{\|\boldsymbol{S}'\|} \right), \\
&\dot{\varphi} = \underbrace{(a_5 c)}_{g_\varphi} \varphi \Rightarrow \boldsymbol{e}_\varphi \overset{\text{def}}{=} \int_0^t \dot{\varphi} \mathbf{1} \, \mathrm{d}t,
\end{aligned} \tag{3.2}$$

where $\boldsymbol{S}$ is the second Piola–Kirchhoff stress, where the normalized concentration of the solute is c, given in molecules per unit volume, where $\boldsymbol{\sigma}'_{\text{crit}} \overset{\text{def}}{=} k_1 \frac{\boldsymbol{\sigma}'}{\|\boldsymbol{\sigma}'\|}$, $\frac{\operatorname{tr} \boldsymbol{\sigma}_{\text{crit}}}{3} \overset{\text{def}}{=} k_2$, k_1 and k_2 being material constants, $\boldsymbol{\sigma}' = \boldsymbol{\sigma} - \frac{\operatorname{tr} \boldsymbol{\sigma}}{3}\mathbf{1}$, $\boldsymbol{S}' = J\boldsymbol{F}^{-1} \cdot \boldsymbol{\sigma}' \cdot \boldsymbol{F}^{-\mathrm{T}}$, $\boldsymbol{S}'_{\text{crit}} = J\boldsymbol{F}^{-1} \cdot \boldsymbol{\sigma}'_{\text{crit}} \cdot \boldsymbol{F}^{-\mathrm{T}}$, where $\boldsymbol{F} = \nabla_X \boldsymbol{x}$ is the deformation gradient, where $J = \det \boldsymbol{F}$ is the Jacobian of the deformation, where the displacement is given by $\boldsymbol{u} = \boldsymbol{x} - \boldsymbol{X}$, where $\boldsymbol{X}$ are referential

[1] Such a law is frame indifferent under rigid body rotations and translations for isotropic $\mathbb{E}$.

coordinates, where $\boldsymbol{x}$ are current coordinates and where a_1 through a_5 are spatially variable material parameters governed by the following activation conditions:

$$
\begin{aligned}
&\text{If } c < c_{\text{crit}} \text{ then } a_1 = a_5 = 0,\\
&\text{If } c \geqslant c_{\text{crit}} \text{ then } a_1 = a_1^*,\ a_5 = a_5^*,\\
&\text{If } \|\boldsymbol{\sigma}'\| \stackrel{\text{def}}{=} \sqrt{\boldsymbol{\sigma}' : \boldsymbol{\sigma}'} < \|\boldsymbol{\sigma}'_{\text{crit}}\| \text{ then } a_2 = a_4 = 0,\\
&\text{If } \|\boldsymbol{\sigma}'\| \stackrel{\text{def}}{=} \sqrt{\boldsymbol{\sigma}' : \boldsymbol{\sigma}'} \geqslant \|\boldsymbol{\sigma}'_{\text{crit}}\| \text{ then } a_2 = a_2^*,\ a_4 = a_4^*,\\
&\text{If } \left|\frac{\operatorname{tr}\boldsymbol{\sigma}}{3}\right| < \left|\frac{\operatorname{tr}\boldsymbol{\sigma}_{\text{crit}}}{3}\right| \text{ then } a_3 = 0,\\
&\text{If } \left|\frac{\operatorname{tr}\boldsymbol{\sigma}}{3}\right| \geqslant \left|\frac{\operatorname{tr}\boldsymbol{\sigma}_{\text{crit}}}{3}\right| \text{ then } a_3 = a_3^*,
\end{aligned}
\tag{3.3}
$$

where c_{crit} is a spatially variable critical (threshold) concentration parameter. The parameters a_1^* through a_5^* are given material parameters that are specified later in the analysis. For further details on these types of phenomenological (damage) formulations, the interested reader is referred to the seminal work of Kachanov [31]. Clearly, further evolution laws can be written for other material property changes, such as $\mathbb{K}$ or $\mathbb{D}_0$, although only changes in $\mathbb{E}$ are considered during the simulations to follow.

3.1. An energy balance including growth

The interconversions of mechanical, thermal and chemical energy are governed by the first law of thermodynamics, which states that the time rate of change of the total energy, $\mathscr{K} + \mathscr{I}$, is equal to the work rate, $\mathscr{P}$, and the net heat supplied, $\mathscr{H} + \mathscr{T}$, i.e.

$$\frac{\mathrm{d}}{\mathrm{d}t}(\mathscr{K} + \mathscr{I}) = \mathscr{P} + \mathscr{H} + \mathscr{T}. \tag{3.4}$$

Consider a subvolume of material contained within Ω, referred to as ω, and

- the kinetic energy given by $\mathscr{K} \stackrel{\text{def}}{=} \int_\omega \frac{1}{2}\rho\dot{\boldsymbol{u}} \cdot \dot{\boldsymbol{u}}\,\mathrm{d}\omega$,
- the stored energy is $\mathscr{I} \stackrel{\text{def}}{=} \int_\omega \rho w\,\mathrm{d}\omega$,
- the rate of work or power of external volumetric ($\rho\boldsymbol{b}$) and surface ($\boldsymbol{\sigma}\cdot\boldsymbol{n}$) forces acting on ω is given by $\mathscr{P} \stackrel{\text{def}}{=} \int_\omega \rho\boldsymbol{b}\cdot\dot{\boldsymbol{u}}\,\mathrm{d}\omega + \int_{\partial\omega}\boldsymbol{\sigma}\cdot\boldsymbol{n}\cdot\dot{\boldsymbol{u}}\,\mathrm{d}a$,
- the heat flow into the volume by conduction is $\mathscr{T} \stackrel{\text{def}}{=} -\int_{\partial\omega}\boldsymbol{q}\cdot\boldsymbol{n}\,\mathrm{d}a = -\int_\omega \nabla_x\cdot\boldsymbol{q}\,\mathrm{d}\omega$,
- the heat generated due to sources, *such as chemical reactions*, is $\mathscr{H} \stackrel{\text{def}}{=} \int_\omega \rho z\,\mathrm{d}\omega$.

Combining the expressions leads to

$$\frac{\mathrm{d}}{\mathrm{d}t}\int_\omega \rho\left(\frac{1}{2}\dot{\boldsymbol{u}}\cdot\dot{\boldsymbol{u}} + w\right)\mathrm{d}\omega = \int_\omega \rho\boldsymbol{b}\cdot\dot{\boldsymbol{u}}\,\mathrm{d}\omega + \int_{\partial\omega}\boldsymbol{\sigma}\cdot\boldsymbol{n}\cdot\dot{\boldsymbol{u}}\,\mathrm{d}a - \int_\omega \nabla_x\cdot\boldsymbol{q}\,\mathrm{d}\omega + \int_\omega \rho z\,\mathrm{d}\omega. \tag{3.5}$$

Converting the first integral to a reference configuration leads to

$$\frac{\mathrm{d}}{\mathrm{d}t}\int_{\omega_0}\rho\left(\frac{1}{2}\dot{\boldsymbol{u}}\cdot\dot{\boldsymbol{u}} + w\right)J\,\mathrm{d}\omega_0 = \int_{\omega_0}\frac{\mathrm{d}}{\mathrm{d}t}(\rho J)\left(\frac{1}{2}\dot{\boldsymbol{u}}\cdot\dot{\boldsymbol{u}} + w\right)\mathrm{d}\omega_0 + \int_{\omega_0}(\rho J)(\ddot{\boldsymbol{u}}\cdot\dot{\boldsymbol{u}} + \dot{w})\,\mathrm{d}\omega_0. \tag{3.6}$$

The third integral in Eq. (3.5) can be converted via Gauss's divergence theorem:

$$\int_{\partial\omega} \boldsymbol{\sigma}\cdot\boldsymbol{n}\cdot\dot{\boldsymbol{u}}\,\mathrm{d}a = \int_{\omega} \nabla_x\cdot(\boldsymbol{\sigma}\cdot\dot{\boldsymbol{u}})\,\mathrm{d}\omega = \int_{\omega} (\nabla_x\cdot\boldsymbol{\sigma}\cdot\dot{\boldsymbol{u}} + \boldsymbol{\sigma}:\nabla_x\dot{\boldsymbol{u}})\,\mathrm{d}\omega. \tag{3.7}$$

Thus, writing all relations in the current configuration, and since the subvolume ω is arbitrary, yields the following local form yields

$$\frac{1}{J}\frac{\mathrm{d}}{\mathrm{d}t}(\rho J)\left(\frac{1}{2}\dot{\boldsymbol{u}}\cdot\dot{\boldsymbol{u}} + w\right) + \rho(\ddot{\boldsymbol{u}}\cdot\dot{\boldsymbol{u}} + \dot{w}) - (\nabla_x\cdot\boldsymbol{\sigma}\cdot\dot{\boldsymbol{u}} + \rho\boldsymbol{b}\cdot\dot{\boldsymbol{u}} + \boldsymbol{\sigma}:\nabla_x\dot{\boldsymbol{u}}) + \nabla_x\cdot\boldsymbol{q} - \rho z = 0. \tag{3.8}$$

Substituting a balance of linear momentum

$$\nabla_x\cdot\boldsymbol{\sigma} + \rho\boldsymbol{b} = \rho\ddot{\boldsymbol{u}}, \tag{3.9}$$

leads to [2]

$$\frac{1}{J}\frac{\mathrm{d}}{\mathrm{d}t}(\rho J)\left(\frac{1}{2}\dot{\boldsymbol{u}}\cdot\dot{\boldsymbol{u}} + w\right) + \rho\dot{w} - \boldsymbol{\sigma}:\nabla_x\dot{\boldsymbol{u}} + \nabla_x\cdot\boldsymbol{q} - \rho z = 0. \tag{3.10}$$

The mass of the solid in the current configuration is given by

$$\int_{\omega}\rho\,\mathrm{d}\omega = \int_{\omega_0}\rho J\,\mathrm{d}\omega_0 \approx \int_{\omega_0}(\rho_0 + \mathscr{F}(c))\,\mathrm{d}\omega_0, \tag{3.11}$$

where $\mathscr{F}(c)$ represents the density changes due to uptake of c. Since the subvolume ω_0 is arbitrary, this implies

$$\rho J \approx \rho_0 + \mathscr{F}(c) \Rightarrow \frac{\mathrm{d}}{\mathrm{d}t}(\rho J) = \dot{\mathscr{F}}(c). \tag{3.12}$$

Finally, we have the following local form,

$$\frac{1}{J}\dot{\mathscr{F}}(c)\left(\frac{1}{2}\dot{\boldsymbol{u}}\cdot\dot{\boldsymbol{u}} + w\right) + \rho\dot{w} - \boldsymbol{\sigma}:\nabla_x\dot{\boldsymbol{u}} + \nabla\cdot\boldsymbol{q} - \rho z = 0. \tag{3.13}$$

We make the following non-hyperelastic, moderate-finite-strain, approximation for the stored energy

$$\rho w = W \approx \tfrac{1}{2}(\boldsymbol{e}-\boldsymbol{\beta}):\mathbb{E}:(\boldsymbol{e}-\boldsymbol{\beta}) + \rho\mathscr{C}\theta, \tag{3.14}$$

where $\boldsymbol{\beta}$ are all of the eigenstrains, which implies, since $\dot{w} = \dot{\left(\frac{W}{\rho}\right)} = \frac{\dot{W}}{\rho} - \frac{W}{\rho^2}\dot{\rho}$,

$$\begin{aligned}\rho\dot{w} = \dot{W} - W\frac{\dot{\rho}}{\rho} = {}& \frac{1}{2}(\boldsymbol{e}-\boldsymbol{\beta}):\dot{\mathbb{E}}:(\boldsymbol{e}-\boldsymbol{\beta}) + (\dot{\boldsymbol{e}}-\dot{\boldsymbol{\beta}}):\mathbb{E}:(\boldsymbol{e}-\boldsymbol{\beta}) + \rho\mathscr{C}\dot{\theta} + \rho\dot{\mathscr{C}}\theta + \dot{\rho}\mathscr{C}\theta \\ & - \frac{\dot{\rho}}{\rho}\left(\frac{1}{2}(\boldsymbol{e}-\boldsymbol{\beta}):\mathbb{E}:(\boldsymbol{e}-\boldsymbol{\beta}) + \rho\mathscr{C}\theta\right),\end{aligned} \tag{3.15}$$

and thus the first law becomes

$$\begin{aligned}\nabla_x\cdot(\mathbb{K}\cdot\nabla_x\theta) = {}& \frac{1}{J}\dot{\mathscr{F}}(c)\left(\frac{1}{2}\dot{\boldsymbol{u}}\cdot\dot{\boldsymbol{u}} + \frac{1}{2\rho}(\boldsymbol{e}-\boldsymbol{\beta}):\mathbb{E}:(\boldsymbol{e}-\boldsymbol{\beta}) + \mathscr{C}\theta\right) + (\dot{\boldsymbol{e}}-\dot{\boldsymbol{\beta}}):\mathbb{E}:(\boldsymbol{e}-\boldsymbol{\beta}) \\ & + \frac{1}{2}(\boldsymbol{e}-\boldsymbol{\beta}):\dot{\mathbb{E}}:(\boldsymbol{e}-\boldsymbol{\beta}) + \rho(\dot{\mathscr{C}}\theta + \mathscr{C}\dot{\theta}) - \rho z - \nabla_x\dot{\boldsymbol{u}}:\mathbb{E}:(\boldsymbol{e}-\boldsymbol{\beta}) \\ & - \frac{1}{2}\left(\frac{\dot{\rho}}{\rho}\right)(\boldsymbol{e}-\boldsymbol{\beta}):\mathbb{E}:(\boldsymbol{e}-\boldsymbol{\beta}),\end{aligned} \tag{3.16}$$

where Fourier's law, $\boldsymbol{q} = -\mathbb{K}\cdot\nabla_x\theta$, has been employed.

[2] Normally, if the mass was conserved, then $\frac{\mathrm{d}}{\mathrm{d}t}(\rho J) = 0$.

Remark. The chemical production of energy at a point is modeled as being related to the change in the rate of damage, $\rho z = \rho\zeta|\dot{\alpha}|$, where ζ is a spatially variable material parameter. The parameter ζ is negative for exothermic reactions and positive for endothermic reactions.

3.2. Mass transfer and reaction–diffusion models

The mass balance for a small diffusing species consists of a storage term ($\dot{c}$), a reaction term ($\dot{s}$), and an inward normal flux term ($-\boldsymbol{G}\cdot\boldsymbol{n}$). Since the domain is undergoing simultaneous finite deformations, consider a control volume for the dilute mass (m) written in the current (deformed) configuration

$$\frac{\mathrm{d}m}{\mathrm{d}t} = \frac{\mathrm{d}}{\mathrm{d}t}\int_{\omega}\mathscr{M}\,\mathrm{d}\omega = \int_{\omega_0}\frac{\mathrm{d}(\mathscr{M}J)}{\mathrm{d}t}\mathrm{d}\omega_0 = \int_{\omega_0}(\dot{\mathscr{M}}J+\mathscr{M}\dot{J})\,\mathrm{d}\omega_0 = \int_{\omega}\left(\dot{\mathscr{M}}+\mathscr{M}\frac{\dot{J}}{J}\right)\mathrm{d}\omega = -\int_{\partial\omega}\boldsymbol{G}\cdot\boldsymbol{n}\,\mathrm{d}a. \tag{3.17}$$

After using the divergence theorem and since the volume ω is arbitrary, one has the local form

$$\dot{\mathscr{M}}+\mathscr{M}\frac{\dot{J}}{J} = -\nabla_x\cdot\boldsymbol{G}. \tag{3.18}$$

We decompose the total dilute mass into two parts, the concentration c and the products of reaction s, $\mathscr{M} = c + s$. It is a classical *stoichiometrically inexact* approximation to assume that the diffusing species reacts (is created or destroyed) in a manner such that the production of the reactant (s) is directly proportional to the concentration (c) of the diffusing species itself [7],

$$s = \tau c. \tag{3.19}$$

Upon substitution of this relation into the conservation law for the diffusing species, one has a diffusion–reaction model in strong form

$$\dot{c}(1+\tau)+c(1+\tau)\frac{\dot{J}}{J} = \nabla_x\cdot(\mathbb{D}_0 e^{-\frac{U}{R\theta}}\cdot\nabla_x c). \tag{3.20}$$

When $\tau > 0$, the diffusing species is destroyed as it reacts, while $\tau < 0$ means that the diffusing species is created as it reacts, i.e. an autocatalytic reaction occurs. In Eq. (3.20), the familiar Arrhenius form $\mathbb{D} = \mathbb{D}_0 e^{-\frac{U}{R\theta}}$ has been used, where $\mathbb{D}_0$ is the diffusivity tensor at a reference temperature and where U is the activation energy per mole of diffusive species, R is the universal gas constant and θ is the temperature.

Remark 1. It is sometimes observed that, in regions of relatively high positive triaxial stress, the diffusion is accelerated, while in regions of high negative triaxial stress, diffusion is decelerated. Diffusion models with explicit pressure dependency will not be considered in the present work, however, we remark that a particularly simple constitutive model to incorporate stress-dependency phenomena is given by a pseudo-Fickian/Arrhenius law, $\boldsymbol{G} = -\mathbb{D}_0 e^{\frac{-U(\sigma)}{R\theta}}\cdot\nabla c$, motivated by thermodynamical arguments found in the classical works of Flynn [10] or Crank [7]. [3]

[3] An additive split for stress dependency of the form $U(\boldsymbol{\sigma}) = U_0 + \widetilde{U}(P)$, where U_0 is a stress-independent reference activation energy and $p = -\frac{\mathrm{tr}\,\boldsymbol{\sigma}}{3}$ is the pressure, has been given in Zohdi [61,62] for certain applications.

Remark 2. It is important to note that instabilities can be induced by diffusion, i.e. a coupled mechano-chemical system can be stable when no diffusion is present and unstable in the presence of diffusion. An indepth mathematical analysis of such effects has been conducted by Markenscoff [33–35].

4. Staggered multifield weak formulations

Staggering schemes are a natural choice for the solution of the multifield system developed thus far. Generally, such approaches proceed, within a discretized time step, by solving each field equation individually, allowing only the corresponding primary field variable to be active. This effectively decouples the system of differential equations. After the solution of each field equation, the primary field variable is updated, and the next field equation is solved in a similar manner, with only the corresponding primary variable being active. Usually, after this process has been applied only once to all of the field equations, the time step is incremented and the procedure is repeated. This non-recursive process can be highly sensitive to the order in which the field variables are determined. For accurate numerical solutions, the approach requires small time steps, primarily because the staggering error accumulates with each passing increment. For details, see Park and Felippa [47], Zienkiewicz [58], Schrefler [51], Lewis et al. [40], Doltsinis [8,9], Piperno [49], Lewis and Schrefler [39] and Le Tallec and Mouro [38]. In an attempt to improve such approaches, a recursive staggering strategy which allowed the adaptive control of time step sizes was developed in Zohdi [59] for a restricted class of coupled geometrically linear/materially nonlinear problems. In that approach, in order to reduce the error within a time step, the staggering methodology was formulated as a recursive fixed-point iteration, whereby the system was repeatedly re-solved until fixed-point type convergence was achieved. A sufficient condition for the convergence of such a fixed-point scheme is that the spectral radius of the coupled operator, which depends on the time step size, must be less than unity. This observation was used to adaptively maximize the time step sizes, while simultaneously controlling the coupled operator's spectral radius, in order to deliver solutions below an error tolerance within a prespecified number of iterations. This recursive staggering error control allowed substantial reduction of computational effort by the adaptive use of large time steps. Furthermore, the recursive process is insensitive to the order in which the individual equations are solved, since it is self-correcting. In the next section, the approach is extended to the wider class of more complicated problems presently considered. For the sake of completeness the presentation is self-contained.

4.1. A recursive algorithm

Within a staggering scheme, we employ a relatively straightforward approach, which is amenable to time step adaptivity is

$$\ddot{\boldsymbol{u}}^{L+1} \approx \frac{\dot{\boldsymbol{u}}^{L+1}-\dot{\boldsymbol{u}}^{L}}{\Delta t} = \frac{\dfrac{\boldsymbol{u}^{L+1}-\boldsymbol{u}^{L}}{\Delta t}-\dot{\boldsymbol{u}}^{L}}{\Delta t} = \frac{\boldsymbol{u}^{L+1}-\boldsymbol{u}^{L}}{(\Delta t)^2}-\frac{\dot{\boldsymbol{u}}^{L}}{\Delta t} = \frac{\boldsymbol{u}^{L+1}}{(\Delta t)^2}-\frac{\boldsymbol{u}^{L}}{(\Delta t)^2}-\frac{\dot{\boldsymbol{u}}^{L}}{\Delta t}, \tag{4.1}$$

where the rate of change of thermal and concentration values are approximated with the same time step size, i.e. $\dot{\theta}^{L+1} \approx \frac{\theta^{L+1}-\theta^{L}}{\Delta t}$ and $\dot{c}^{L+1} \approx \frac{c^{L+1}-c^{L}}{\Delta t}$. During the staggering process, the geometric configuration of the system is frozen during each iteration, and is updated only at the end of a system recursion. This is essentially an "updated Lagrangian" formulation, where all variables are referred to the last calculated configuration as opposed to a "total Lagrangian" formulation where all variables are referred to the initial configuration. In this particular case, the last calculated configuration is the previously computed one within the staggering scheme. Algorithmically, employing weak formulations, the staggering scheme is as follows:

($\bigstar$) At a time step(L): Start an internal iteration$I = 0$

($\bigstar\bigstar$) Update geometrical configuration: $\Omega^{L+1,I} = \Omega^{L+1,I-1}$

Mass balance of diffusing species:

Find $c^{L+1,I+1} \in U_c(\Omega^{L+1,I}), c^{L+1,I+1}|_{\Gamma_c} = C, \quad$ such that $\forall v \in V_c(\Omega^{L+1,I}), \ v|_{\Gamma_c} = 0$

$$\int_{\Omega^{L+1,I}} \nabla_x v \cdot \mathbb{D}_0^{L+1,I} e^{-\frac{U}{R\theta^{L+1,I}}} \cdot \nabla_x c^{L+1,I+1} \, \mathrm{d}\Omega$$

$$+ \int_{\Omega^{L+1,I}} v(1+\tau) c^{L+1,I+1} \left(\frac{1}{\Delta t} + \frac{\dot{J}^{L+1,I}}{J^{L+1,I}} \right) \mathrm{d}\Omega = \int_{\Omega^{L+1,I}} v \frac{(1+\tau)}{\Delta t} c^L \mathrm{d}\Omega + \int_{\Gamma_G} v \boldsymbol{G}^{L+1} \cdot \boldsymbol{n} \, \mathrm{d}A.$$

Compute reactions: (Integrate evolution equations)

$$\dot{\alpha}^{L+1,I+1} = g_\alpha^{L+1,I+\frac{1}{3}} \alpha^{L+1,I+1} \Rightarrow \alpha^{L+1,I+1} = \alpha^L e^{g_\alpha^{L+1,I+\frac{1}{3}} \Delta t^{L+1}}, \tag{4.2}$$

$$\dot{\lambda}^{L+1,I+1} = g_\lambda^{L+1,I+\frac{1}{3}} \lambda^{L+1,I+1} \Rightarrow \lambda^{L+1,I+1} = \lambda^L e^{g_\lambda^{L+1,I+\frac{1}{3}} \Delta t^{L+1}} \Rightarrow \boldsymbol{e}_\lambda^{L+1,I+1},$$

$$\dot{\varphi}^{L+1,I+1} = g_\varphi^{L+1,I+\frac{1}{3}} \varphi^{L+1,I+1} \Rightarrow \varphi^{L+1,I+1} = \varphi^L e^{g_\varphi^{L+1,I+\frac{1}{3}} \Delta t^{L+1}} \Rightarrow \boldsymbol{e}_\varphi^{L+1,I+1},$$

where

$$g^{L+1,I+\frac{1}{3}} \stackrel{\text{def}}{=} g(c^{L+1,I+1}, \theta^{L+1,I}, \boldsymbol{u}^{L+1,I}),$$

$$g^{L+1,I+\frac{2}{3}} \stackrel{\text{def}}{=} g(c^{L+1,I+1}, \theta^{L+1,I+1}, \boldsymbol{u}^{L+1,I}),$$

$$g^{L+1,I+1} \stackrel{\text{def}}{=} g(c^{L+1,I+1}, \theta^{L+1,I+1}, \boldsymbol{u}^{L+1,I+1}).$$

Compute heat generation: $(\rho z)^{L+1,I+1} = \zeta \rho^{L+1,I} \dot{\alpha}^{L+1,I+1},$

with the algorithm proceeding with

Energy equation:

Find $\theta^{L+1,I+1} \in U_\theta(\Omega^{L+1,I}), \theta^{L+1,I+1}|_{\Gamma_\theta^{L+1,I}} = \Theta^{L+1} \quad$ such that $\forall v \in V_\theta(\Omega^{L+1,I}), \ v|_{\Gamma_\theta^{L+1,I}} = 0$

$$\int_{\Omega^{L+1,I}} \nabla_x v \cdot \mathbb{K}^{L+1,I+1} \cdot \nabla_x \theta^{L+1,I+1} \, \mathrm{d}\Omega + \frac{1}{\Delta t} \int_{\Omega^{L+1,I}} v \rho^{L+1,I} \mathscr{C}^{L+1,I+1} \theta^{L+1,I+1} \, \mathrm{d}\Omega$$

$$= \frac{1}{\Delta t} \int_{\Omega^{L+1,I}} v \rho^{L+1,I} \mathscr{C}^{L+1,I+1} \theta^L \, \mathrm{d}\Omega - \int_{\Omega^{L+1,I}} v \left(\rho^{L+1,I} \dot{\mathscr{C}}^{L+1,I+1} + \frac{1}{J^{L+1,I}} \dot{\mathscr{F}}(c^{L+1,I+1}) \mathscr{C}^{L+1,I+1} \right) \theta^{L+1,I+1} \, \mathrm{d}\Omega$$

$$+ \int_{\Omega^{L+1,I}} v (\rho z)^{L+1,I+1} \, \mathrm{d}\Omega + \int_{\Gamma_q^{L+1,I}} v \boldsymbol{q}^{L+1} \cdot \boldsymbol{n} \, \mathrm{d}A$$

$$- \int_{\Omega^{L+1,I}} v \left(\left(\dot{\boldsymbol{e}}^{L+1,I} - \dot{\boldsymbol{\beta}}^{L+1,I+\frac{1}{3}} \right) : \mathbb{E}^{L+1,I+1} : \left(\boldsymbol{e}^{L+1,I} - \boldsymbol{\beta}^{L+1,I+\frac{1}{3}} \right) \right) \mathrm{d}\Omega$$

$$- \int_{\Omega^{L+1,I}} v \left(\frac{1}{2} \left(\boldsymbol{e}^{L+1,I} - \boldsymbol{\beta}^{L+1,I+\frac{1}{3}} \right) : \dot{\mathbb{E}}^{L+1,I+1} : \left(\boldsymbol{e}^{L+1,I} - \boldsymbol{\beta}^{L+1,I+\frac{1}{3}} \right) \right) \mathrm{d}\Omega$$

$$+ \int_{\Omega^{L+1,I}} v \left(\nabla_x \dot{\boldsymbol{u}}^{L+1,I} : \left(\mathbb{E}^{L+1,I+1} : \left(\boldsymbol{e}^{L+1,I} - \boldsymbol{\beta}^{L+1,I+\frac{1}{3}} \right) \right) \right) \mathrm{d}\Omega$$

$$+\int_{\Omega^{L+1,I}} v\left(\frac{\dot{\rho}^{L+1,I}}{\rho^{L+1,I}}\frac{1}{2}\left(\boldsymbol{e}^{L+1,I}-\boldsymbol{\beta}^{L+1,I+\frac{1}{3}}\right):\mathbb{E}^{L+1,I+1}:\left(\boldsymbol{e}^{L+1,I}-\boldsymbol{\beta}^{L+1,I+\frac{1}{3}}\right)\right)\mathrm{d}\Omega$$

$$+\int_{\Omega^{L+1,I}} v\frac{1}{J^{L+1,I}}\dot{\mathscr{F}}(c^{L+1,I+1})\left(\frac{1}{2}\dot{\boldsymbol{u}}^{L+1,I}\cdot\dot{\boldsymbol{u}}^{L+1,I}+\frac{1}{2\rho^{L+1,I}}(\boldsymbol{e}^{L+1,I}-\boldsymbol{\beta}^{L+1,I}):\mathbb{E}^{L+1,I+1}:(\boldsymbol{e}^{L+1,I}-\boldsymbol{\beta}^{L+1,I})\right)\mathrm{d}\Omega.$$

Balance of momentum:

Find $\boldsymbol{u}^{L+1,I+1}\in\boldsymbol{U}_u(\Omega^{L+1,I}),\boldsymbol{u}^{L+1,I+1}|_{\Gamma_u^{L+1,I}}=\boldsymbol{d}^{L+1}$ such that $\forall\boldsymbol{v}\in\boldsymbol{V}_u(\Omega^{L+1,I}),\ \boldsymbol{v}|_{\Gamma_u^{L+1,I}}=\boldsymbol{0}$

$$\int_{\Omega^{L+1,I}}\nabla_x\boldsymbol{v}:\alpha^{L+1,I+1}\mathbb{E}_0:\left(\nabla_x\boldsymbol{u}^{L+1,I+1}-\frac{1}{2}(\nabla_x\boldsymbol{u}^{L+1,I})^{\mathrm{T}}\cdot\nabla_x\boldsymbol{u}^{L+1,I}-\boldsymbol{\beta}^{L+1,I+\frac{2}{3}}\right)\mathrm{d}\Omega$$

$$+\int_{\Omega^{L+1,I}}\rho^{L+1,I}\frac{\boldsymbol{u}^{L+1,I+1}}{(\Delta t)^2}\cdot\boldsymbol{v}\,\mathrm{d}\Omega-\int_{\Omega^{L+1,I}}\rho^{L+1,I}\left(\frac{\boldsymbol{u}^{L}}{(\Delta t)^2}+\frac{\dot{\boldsymbol{u}}^{L}}{\Delta t}\right)\cdot\boldsymbol{v}\,\mathrm{d}\Omega$$

$$-\int_{\Omega^{L+1,I}}\boldsymbol{f}^{L+1,I}\cdot\boldsymbol{v}\,\mathrm{d}\Omega-\int_{\Gamma_t^{L+1,I}}\boldsymbol{t}^{L+1,I}\cdot\boldsymbol{v}\,\mathrm{d}A=0.$$

Check for convergence:

$$\frac{\|\boldsymbol{u}^{L+1,I+1}-\boldsymbol{u}^{L+1,I}\|_{\boldsymbol{L}^1(\Omega^{L+1,I})}}{\|\boldsymbol{u}^{L+1,I+1}\|_{\boldsymbol{L}^1(\Omega^{L+1,I})}}\leqslant\mathrm{TOL}_u,$$

$$\frac{\|c^{L+1,I+1}-c^{L+1,I}\|_{\boldsymbol{L}^1(\Omega^{L+1,I})}}{\|c^{L+1,I+1}\|_{\boldsymbol{L}^1(\Omega^{L+1,I})}}\leqslant\mathrm{TOL}_c,$$

$$\frac{\|\theta^{L+1,I+1}-\theta^{L+1,I}\|_{\boldsymbol{L}^1(\Omega^{L+1,I})}}{\|\theta^{L+1,I+1}\|_{\boldsymbol{L}^1(\Omega^{L+1,I})}}\leqslant\mathrm{TOL}_\theta.$$

If tolerances not met then $I=I+1$, go to ($\bigstar\bigstar$)

If tolerances met then increment time: $L=L+1$ and update all variables, go to ($\bigstar$).

(4.3)

Here $U_c(\Omega)$, $U_\theta(\Omega)$ and $\boldsymbol{U}_u(\Omega)$ are spaces of admissible trial functions, while $V_c(\Omega)$, $V_\theta(\Omega)$ and $\boldsymbol{V}_u(\Omega)$ are spaces of admissible test functions. For most loading cases and data these spaces will correspond to $H^1(\Omega)$ and $\boldsymbol{H}^1(\Omega)$. In an abstract setting, one can consider the following staggering solution strategy where only the underlined variable is allowed to be active, the corresponding field equations solved, the active variable updated, and the process repeated for the next field equation:

$$\begin{aligned}
&\mathscr{A}_1(\underline{c^{I+1}},\alpha^I,\boldsymbol{e}_\lambda^I,\boldsymbol{e}_\varphi^I,\theta^I,\boldsymbol{u}^I)=\mathscr{F}_1(c^I,\alpha^I,\boldsymbol{e}_\lambda^I,\boldsymbol{e}_\varphi^I,\theta^I,\boldsymbol{u}^I)\quad\text{(Mass transfer)},\\
&\mathscr{A}_2(c^{I+1},\underline{\alpha^{I+1}},\boldsymbol{e}_\lambda^I,\boldsymbol{e}_\varphi^I,\theta^I,\boldsymbol{u}^I)=\mathscr{F}_2(c^{I+1},\alpha^I,\boldsymbol{e}_\lambda^I,\boldsymbol{e}_\varphi^I,\theta^I,\boldsymbol{u}^I)\quad\text{(Degradation)},\\
&\mathscr{A}_3(c^{I+1},\alpha^{I+1},\underline{\boldsymbol{e}_\lambda^{I+1}},\boldsymbol{e}_\varphi^I,\theta^I,\boldsymbol{u}^I)=\mathscr{F}_3(c^{I+1},\alpha^{I+1},\boldsymbol{e}_\lambda^I,\boldsymbol{e}_\varphi^I,\theta^I,\boldsymbol{u}^I)\quad\text{(Dev. eigenstrains)},\\
&\mathscr{A}_4(c^{I+1},\alpha^{I+1},\boldsymbol{e}_\lambda^{I+1},\underline{\boldsymbol{e}_\varphi^{I+1}},\theta^I,\boldsymbol{u}^I)=\mathscr{F}_4(c^{I+1},\alpha^{I+1},\boldsymbol{e}_\lambda^{I+1},\boldsymbol{e}_\varphi^I,\theta^I,\boldsymbol{u}^I)\quad\text{(Dil. eigenstrains)},\\
&\mathscr{A}_5(c^{I+1},\alpha^{I+1},\boldsymbol{e}_\lambda^{I+1},\boldsymbol{e}_\varphi^{I+1},\underline{\theta^{I+1}},\boldsymbol{u}^I)=\mathscr{F}_5(c^{I+1},\alpha^{I+1},\boldsymbol{e}_\lambda^{I+1},\boldsymbol{e}_\varphi^{I+1},\theta^I,\boldsymbol{u}^I)\quad\text{(Energy)},\\
&\mathscr{A}_6(c^{I+1},\alpha^{I+1},\boldsymbol{e}_\lambda^{I+1},\boldsymbol{e}_\varphi^{I+1},\theta^{I+1},\underline{\boldsymbol{u}^{I+1}})=\mathscr{F}_6(c^{I+1},\alpha^{I+1},\boldsymbol{e}_\lambda^{I+1},\boldsymbol{e}_\varphi^{I+1},\theta^{I+1},\boldsymbol{u}^I)\quad\text{(Momentum)}.
\end{aligned}\tag{4.4}$$

Remark I. Consistent with the fully staggered solution approach introduced in Box (4.2), we freeze the g_α, g_λ and g_φ, using the most current state variable values, and integrate analytically.

Remark II. Writing the system in the form presented leads to algebraic systems which are symmetric and positive definite. Therefore, somewhat standard iterative solvers, such as the preconditioned Conjugate Gradient Method, can be used. Such solvers are highly advantageous since any starting solution, from a previous time step or staggered iteration can be used as the first guess in the solution procedure, thus providing a "head start" in the process.

4.2. Convergence and contraction-mapping time stepping control

Consider the general abstract equation

$$\mathscr{A}(\boldsymbol{w}) = \mathscr{F}, \tag{4.5}$$

where $\boldsymbol{w}$ represents all of the fields in the analysis:

$$\boldsymbol{w} \stackrel{\text{def}}{=} (c, \alpha, \boldsymbol{e}_\lambda, \boldsymbol{e}_\varphi, \theta, \boldsymbol{u}), \tag{4.6}$$

It is advantageous to write this in the form

$$\boldsymbol{\Pi}(\boldsymbol{w}) = \mathscr{A}(\boldsymbol{w}) - \mathscr{F} = \mathscr{G}(\boldsymbol{w}) - \boldsymbol{w} + \boldsymbol{r} = \boldsymbol{0}. \tag{4.7}$$

A straightforward fixed point iterative scheme is

$$\mathscr{G}(\boldsymbol{w}^{I-1}) + \boldsymbol{r} = \boldsymbol{w}^I. \tag{4.8}$$

The convergence of such a scheme is dependent on the behavior of $\mathscr{G}$. Namely, a sufficient condition for convergence is that $\mathscr{G}$ is a contraction mapping for all $\boldsymbol{w}^I$, $I = 1, 2, 3, \ldots$ Convergence of the iteration can be studied by defining the error vector $\varepsilon_I = \boldsymbol{w}^I - \boldsymbol{w}$. A necessary condition for convergence is iterative self-consistency, i.e. the exact solution must be represented by the scheme $\mathscr{G}(\boldsymbol{w}) + \boldsymbol{r} = \boldsymbol{w}$. Enforcing this condition, a sufficient condition for convergence is the existence of a contraction mapping

$$\|\varepsilon_I\| = \|\boldsymbol{w}^I - \boldsymbol{w}\| = \|\mathscr{G}(\boldsymbol{w}^{I-1}) - \mathscr{G}(\boldsymbol{w})\| \leqslant \eta \|\boldsymbol{w}^{I-1} - \boldsymbol{w}\|, \tag{4.9}$$

where, if $\eta < 1$ for each iteration I, then $\varepsilon_I \to \boldsymbol{0}$ for any arbitrary starting solution $\boldsymbol{w}^{I=0}$ as $I \to \infty$. Therefore, unconditional convergence is attained if for $\boldsymbol{w}^I$, $I = 1, 2, 3, \ldots$, $\eta^I < 1$. This type of convergence criteria is common for linear iterative (Gauss–Jacobi–Seidel) solution methods of relaxation type [6,11,53,54,57]. For reviews of nonlinear techniques, we refer the reader to Perron [48], Ostrowski [45,46], Ortega and Rockoff [44], Kitchen [32] or Ames [4]. The algorithm outlined in Eqs. (4.2) and (4.3) can be considered as fixed-point scheme, whose convergence within each time step is dependent on the time step size itself. The step size can be manipulated, enlarged or reduced, to induce the desired rates of convergence within a time step, in order to achieve an error tolerance within a prespecified number of iterations. Following the approach in Zohdi [59,60], one approximates the contraction constant $\eta \approx S\Delta t$, where one expects the error within an iteration to behave according to $(S\Delta t)^I \varepsilon_0 = \varepsilon_I$, $I = 1, 2, \ldots$, where ε_0 is the initial error and S is a function intrinsic to the system. Our target or ideal condition is to meet an error tolerance in a given number of iterations, not more, and not less. One writes this in the following approximate form, $(S\Delta t_{\text{tol}})^{I_d} \varepsilon_0 = \text{TOL}$, where I_d is the number of desired iterations. Therefore, if the error tolerance is not met in a desired number of iterations, the contraction constant η is too large. Accordingly, one can solve for a new smaller step size, under the assumption that S is constant [4]

[4] The assumption that S is constant is not overly severe, since the time steps are to be recursively refined and unrefined.

$$\Delta t_{\text{tol}} = \Delta t \left(\frac{\left(\dfrac{\text{TOL}}{\varepsilon_0} \right)^{\frac{1}{I_d}}}{\left(\dfrac{\varepsilon_I}{\varepsilon_0} \right)^{\frac{1}{7}}} \right). \tag{4.10}$$

Clearly, the expression in Eq. (4.10) can be used for time step enlargement, if convergence is met in less than I_d iterations. One sees that if $\varepsilon_{I_d} > \varepsilon_{\text{tol}}$ and $I = I_d$, then the expression in Eq. (4.10) collapses to a ratio of the error tolerance to the achieved level of iterative error after I_d iterations, $\Delta t_{\text{tol}} = \Delta t \left(\frac{\text{TOL}}{\varepsilon_{I_d}} \right)^{I_d}$, and thus the step size will be scaled by the ratio of the error to the tolerance. For the multifield system, we define the normalized errors within each time step (L), for the three primary fields, [5]

$$\begin{aligned}
\varepsilon_{uI} &\stackrel{\text{def}}{=} \frac{\left\| \boldsymbol{u}^{L+1,I} - \boldsymbol{u}^{L+1,I-1} \right\|_{\boldsymbol{L}^1(\Omega)}}{\left\| \boldsymbol{u}^{L+1,I} \right\|_{\boldsymbol{L}^1(\Omega)}}, \\
\varepsilon_{cI} &\stackrel{\text{def}}{=} \frac{\left\| c^{L+1,I} - c^{L+1,I-1} \right\|_{\boldsymbol{L}^1(\Omega)}}{\left\| c^{L+1,I} \right\|_{\boldsymbol{L}^1(\Omega)}}, \\
\varepsilon_{\theta I} &\stackrel{\text{def}}{=} \frac{\left\| \theta^{L+1,I} - \theta^{L+1,I-1} \right\|_{\boldsymbol{L}^1(\Omega)}}{\left\| \theta^{L+1,I} \right\|_{\boldsymbol{L}^1(\Omega)}},
\end{aligned} \tag{4.11}$$

and their corresponding violation ratios

$$\psi_{uI} \stackrel{\text{def}}{=} \frac{\varepsilon_{uI}}{\text{TOL}_u}, \quad \psi_{\theta I} \stackrel{\text{def}}{=} \frac{\varepsilon_{\theta I}}{\text{TOL}_\theta}, \quad \psi_{cI} \stackrel{\text{def}}{=} \frac{\varepsilon_{cI}}{\text{TOL}_c}. \tag{4.12}$$

One then determines the maximum violation $\Psi_I \stackrel{\text{def}}{=} \max(\psi_{uI}, \psi_{cI}, \psi_{\theta I})$ and a minimum scaling factor $\Phi_I \stackrel{\text{def}}{=} \min(\phi_{uI}, \phi_{cI}, \phi_{\theta I})$ from

$$\phi_{uI} \stackrel{\text{def}}{=} \left(\frac{\left(\dfrac{\text{TOL}_u}{\varepsilon_{u0}} \right)^{\frac{1}{I_d}}}{\left(\dfrac{\varepsilon_{uI}}{e_u^0} \right)^{\frac{1}{7}}} \right), \quad \phi_{cI} \stackrel{\text{def}}{=} \left(\frac{\left(\dfrac{\text{TOL}_c}{\varepsilon_{c0}} \right)^{\frac{1}{I_d}}}{\left(\dfrac{\varepsilon_{cI}}{\varepsilon_{c0}} \right)^{\frac{1}{7}}} \right), \quad \phi_{\theta I} \stackrel{\text{def}}{=} \left(\frac{\left(\dfrac{\text{TOL}_\theta}{\varepsilon_{\theta 0}} \right)^{\frac{1}{I_d}}}{\left(\dfrac{\varepsilon_{\theta I}}{\varepsilon_{\theta 0}} \right)^{\frac{1}{7}}} \right). \tag{4.13}$$

Thereafter, the following criteria for temporal adaptivity is adopted:

If tolerances met(ψ_{uI} and $\psi_{\theta I}$ and $\psi_{cI} \leqslant 1$) and $I < I_d$ then:
- (a) Construct new time step: $\Delta t = \Phi_I \Delta t$
- (b) Select minimum: $\Delta t = \text{MIN}(\Delta t^{\text{lim}}, \Delta t)$
- (c) Step time forward: $t = t + \Delta t$and start at time step$(L+1)$

If any tolerance not met(ψ_{uI} or $\psi_{\theta I}$ or $\psi_{cI} > 1$) or $I = I_d$ then:
- (a) Construct new time step: $\Delta t = \Phi_{I_d} \Delta t$
- (b) Select minimum: $\Delta t = \text{MIN}(\Delta t^{\text{lim}}, \Delta t)$
- (c) Restart at old time

(4.14)

[5] The other quantities, α, $\boldsymbol{e}_\lambda$, and $\boldsymbol{e}_\varphi$ are controlled by the three primary fields $(c, \theta, \boldsymbol{u})$, thus we monitor only their convergence.

The overall goal is to deliver solutions where staggering (incomplete coupling) error is controlled and the temporal discretization accuracy dictates the upper limits on the time step size ($\Delta t^{\lim}$).

5. Numerical experiments

To illustrate the algorithm, we considered a microscale cube of matrix material, with dimensions 10^{-4} m$\times 10^{-4}$ m$\times 10^{-4}$ m, with embedded randomly distributed inhomogeneities. The various physical properties of the two materials are shown in Table 1, and correspond to a commonly used lightweight aluminum matrix-boron particle industrial composite. We consider a set of topological microstructural variables which can be conveniently parametrized by a generalized "ellipsoid"

$$\left(\frac{|x-x_0|}{r_1}\right)^{s_1}+\left(\frac{|y-y_0|}{r_2}\right)^{s_2}+\left(\frac{|z-z_0|}{r_3}\right)^{s_3}=1. \tag{5.1}$$

The types of suspensions to be introduced in the matrix binder can be controlled by (1) the polynomial order, s_1, s_2 and s_3, where values of $s<1$ produce non-convex shapes, $s=1$ produce convex eight-sided diamond shapes, $s=2$ standard ellipsoids and $s>2$ values produce "blocklike" shapes, (2) the aspect ratios defined by $\mathrm{AR}\stackrel{\mathrm{def}}{=}\frac{r_1}{r_2}=\frac{r_1}{r_3}$, where $r_2=r_3$, $\mathrm{AR}>1$ for prolate geometries and $AR<1$ for oblate shapes and (3) the volume fractions, via particle/sample size ratio, which is defined via a subvolume size $V\stackrel{\mathrm{def}}{=}\frac{L\times L\times L}{N}$, where N is the number of particles in the entire sample and where $L=10^{-4}$ m is the length of the (cubical) sample, $L\times L\times L$. A generalized diameter is defined, $d=2r$, which is the diameter of the smallest sphere

Table 1
Material properties used in the computational examples

Material property	Matrix	Particles
Mechanical		
κ (GPa)	77.9	230.0
μ (GPa)	25.9	172.0
γ (1/°K)	9.71×10^{-6}	8.92×10^{-6}
Thermal		
K (J/s m °K)	237	148
ρ (kg/m^3)	2700.84	2330.28
$\mathscr{C}$ (J/kg °K)	903	712
Diffusive		
D_0 (m/s^2)	1.0×10^{-6}	1.0×10^{-7}
U (kN m/mole)	142	300
τ (1/s)	5.0×10^{-2}	1.0×10^{-2}
Damage evolution		
a_1^* (m^3/molecules s)	-7.3×10^{-8}	-3.0×10^{-9}
a_2^* (m^3/molecules s)	-7.3×10^{-8}	-3.0×10^{-9}
a_3^* (m^3/molecules s)	-7.3×10^{-8}	-3.0×10^{-9}
a_4^* (1/s)	6.27×10^{-10}	3.15×10^{-10}
a_5^* (1/s)	6.27×10^{-11}	3.15×10^{-11}
k_1 (MPa)	120	3000
k_2 (MPa)	120	3000
c_{crit} (molecules/m^3)	0.0	0.0
ζ (N m)	-1×10^{11}	-5×10^{11}

that can enclose a single particle of possibly non-spherical shape. The ratio between the generalized diameter and the subvolume are related by $\xi \stackrel{\text{def}}{=} \frac{r}{V^{\frac{1}{3}}}$. In order to illustrate the behavior we used the disk-like microstructure shown in Fig. 2. For any microstructural combination, volume fractions, phase contrasts, etc..., the samples must be tested and enlarged, holding the volume fraction constant, but increasing the number of particles, for example from $2, 4, \ldots$,etc., ..., until the macroscopic results stabilize. Approximately a 20 particle sample gave relatively stable results. A more detailed and rigorous analysis of size effects for such systems is beyond the scope of this presentation. The reader is referred to the following series of works Huet [25–29], Huet et al. [30], Guidoum and Navi [13], Amieur et al. [1], Guidoum [14], Amieur [2] Hazanov and Huet [15], Hazanov and Amieur [16], Amieur et al. [3] and Huet [22–24], as well as some recent work of the author [59,63–66].

Over the course of such tests the finite element meshes were repeatedly refined, and a mesh density of approximately $9\times9\times9$ trilinear hexahedra (approximately 800–1000 degrees of freedom (DOF) for the diffusion–reaction and energy balance equations, and between 2200 and 3000 DOF for the vector-valued balance of momentum) *per particle* was found to deliver mesh independent results. Therefore, for example for a 10 particle test, 8000 DOF were needed for the diffusion–reaction and energy balance equation, and 24,000 DOF for the balance of momentum equation, for 20 particles, 15,625 DOF/46,875 DOF, etc. During the computations, a "2/5" Gauss rule was used, whereby elements containing material discontinuities had increased Gauss rules ($5\times5\times5$) to enhance the resolution of the internal geometry, while elements with no material discontinuities had the nominal $2\times2\times2$ rule. The numerical resolution of the microstructure is shown in Fig. 2, for a topological exponent of $s_1 = s_2 = s_3 = 2$ for oblate spheroids. For related work in the optimization of the material microstructure, controlling the parameters such as s, see Zohdi [63,65,66].

The boundary conditions for the cubical domain were: (1) $c|_{\partial\Omega} = C = 1$, $c(\boldsymbol{x}, t = 0) = 0$, (2) $\theta|_{\partial\Omega} = \Theta = 30°$ Celcius $= 303.13°$ Kelvin, $\theta(\boldsymbol{x}, t = 0) = 0°$ Celcius and (3) $\boldsymbol{u}|_{\partial\Omega} = \frac{t}{T}\mathscr{E}\cdot\boldsymbol{X}$, $\mathscr{E}_{ij} = 0.02$, $i, j = 1, 2, 3$, where $\boldsymbol{X}$ is a referential position vector to the boundary of the cube, t is the time, and T is the total simulation time. The material parameters, *selected only for the purposes of numerical experiment*, are shown in Table 1. From a practical engineering point of view, macroscopic quantities, which are volumetrically averaged outcomes of the simulated microstructural events, are of interest. Such quantities include, (1) the mechanical response, $\langle\boldsymbol{\sigma}\rangle_{\Omega}$, (2) the average change in the material, for example damage, $\langle\alpha\rangle_{\Omega}$, (3) the average

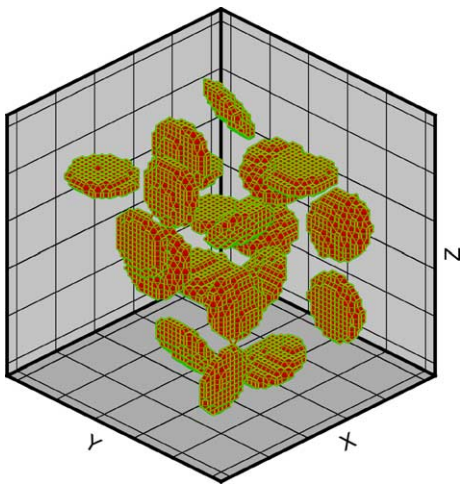

Fig. 2. The numerical resolution of $s_1 = s_2 = s_3 = 2$ particles, with $\xi = 0.375$, and an aspect ratio of $\frac{1}{3}$, i.e. $r_1 = \frac{1}{3}r_2 = \frac{1}{3}r_3$ resulting in a volume fraction of $v_2 \approx 0.076$ (20 particles shown).

temperature, $\langle\theta\rangle_\Omega$, and (4) the average concentration $\langle c\rangle_\Omega$. The deterioration rates of all material parameters other than $\mathbb{E}$ such as $\mathbb{K}$, $\mathbb{D}_0$, etc., were set to zero in the present simulations. Clearly, in this external pure displacement controlled regime, the stresses will relax over time, since the material stiffness is deteriorating in the interior.

The algorithmic staggering tolerance was set to $\max(\varepsilon_u, \varepsilon_\theta, \varepsilon_c) \leqslant 0.0001$ for the normalized/global error control. The designated maximum number of internal iterations, I_d, was set to five. The starting time step size was $\Delta t = 10^3$ s. In order to smoothly refine and unrefine the time steps, the adjustments were bounded *between successive time steps* (L) to be $0.9 < \frac{\Delta t^{L+1}}{\Delta t^L} \leqslant 1.1$. The total simulation time was set to 1 year. *For the purposes of numerical experiment only*, the damage rate parameters were chosen such that for a material point undergoing constant damage at unit concentration, with no stress, after one year $\alpha(t = T) = 0.1 = e^{a_1^* t}$, $T = 31,536,000$ s, which led to $a_1^* = -7.3 \times 10^{-8}$ (m^3/molecules s). This rate was used for the matrix. For the particulate material, we set the rate parameter to be significantly smaller, $a_1^* = -3 \times 10^{-9}$

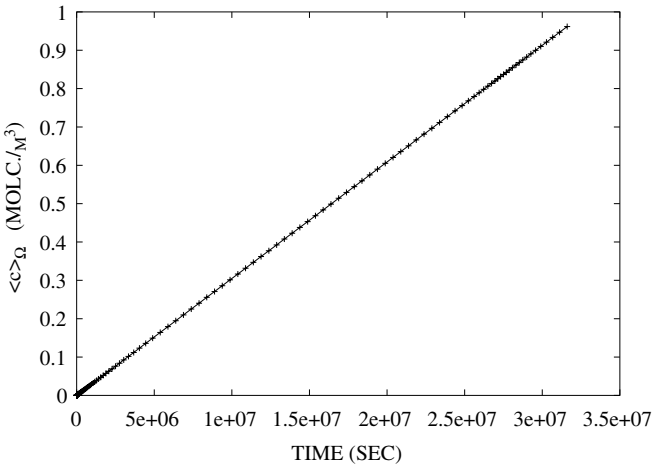

Fig. 3. The volumetric average of the concentration over time.

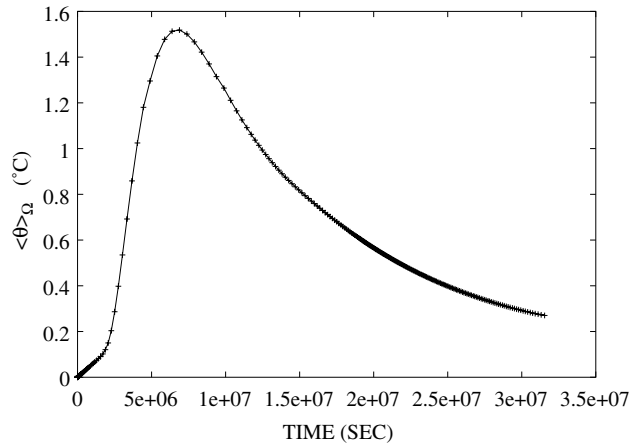

Fig. 4. The volumetric average of the temperature over time.

(m^3/molecules s). These values were also selected for the a_2^* and a_3^* rates as well. The deterioration rates of all material parameters other than $\mathbb{E}$, such as $\mathscr{C}$, $\mathbb{K}$, $\mathbb{D}_0$, etc., were set to zero. For the deviatoric eigenstrain, the rate coefficient a_4^* was calibrated in such a way that $\lambda = 0.02$ in the matrix and $\lambda = 0.01$ in the particle, for constant $\dot{\lambda}$'s, at $t = T$. A value of one-tenth was used for the dilatational eigenstrain. Finally, the function for the changes in density due to the uptake of the diffusing species was modeled as $\mathscr{F}(c) \approx ac$, with $a = 0.1$ kg/molecule. The time step limit size was set to 5×10^5 s, which was set as the upper bound for reasons of truncation error control. The total number of system solves needed was 462, as opposed to 31,536, had the system been solved non-recursively with no time step adaptation. Figs. 3–8 illustrate the results for the major quantities of interest. The volumetric average of the concentration (Fig. 3) exhibits a quasilinear growth over time. The volumetric average of the temperature (Fig. 4) exhibits a nonlinear, non-monotone, behavior over time, representing initial heating then cooling off. The volumetric average of the

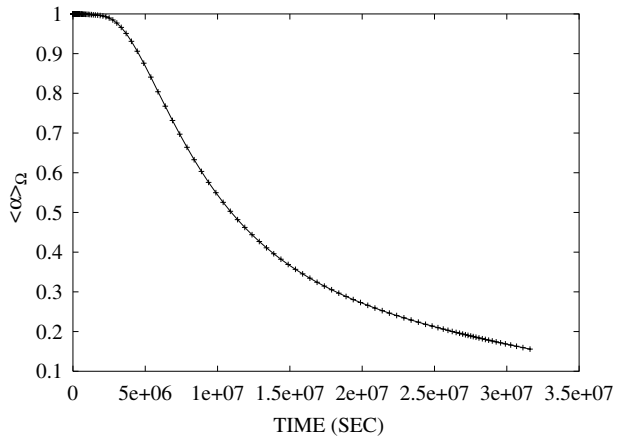

Fig. 5. The volumetric average of the degradation over time.

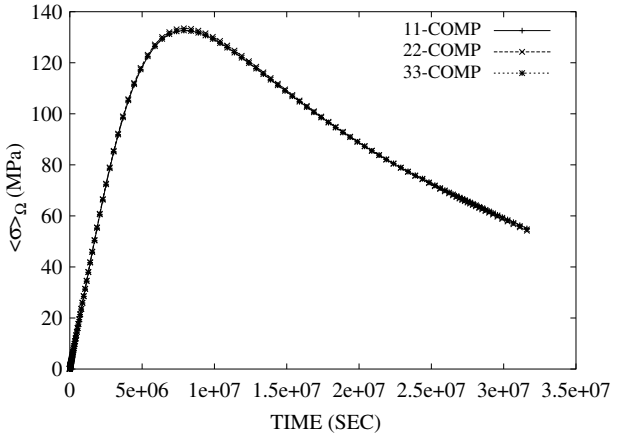

Fig. 6. The volumetric average of the normal stresses over time.

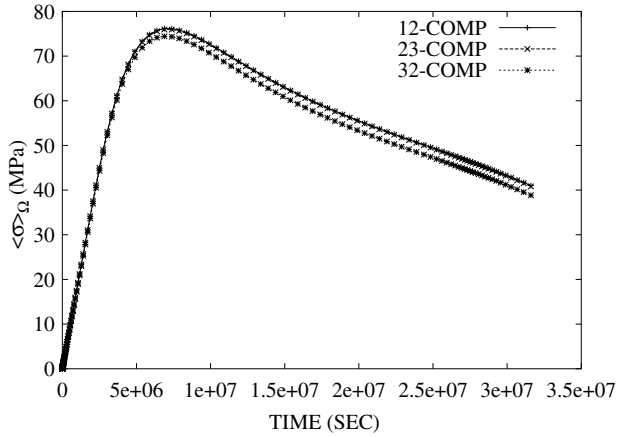

Fig. 7. The volumetric average of the shear stresses over time.

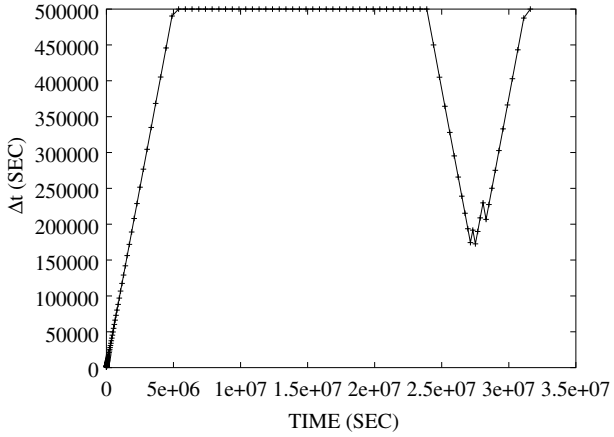

Fig. 8. The adapted time step sizes over time.

damage is also highly nonlinear (Fig. 5), and the stresses growth, then relax in a manner that is characteristic of solids undergoing softening (Figs. 6 and 7). In Fig. 7 minor anisotropic texture is exhibited, indicating that the sample is slightly non-statistically representative. Finally, Fig. 8 shows the variation in the time step sizes to meet the staggering and discretization error requirements. A spatial time history of the degradation throughout the solid is shown in Figs. 9 and 10.

6. Concluding remarks

In this work, the (staggering) error due to incompletely resolving the coupling between multifield equations, describing time-dependent thermo-chemo-mechanical processes in solids possessing irregular heterogeneous microstructure, was characterized in such a way to be amenable to a relatively simple method of adaptive control. A solution strategy was developed, whereby the time step size was manipulated, enlarged or reduced, to control the contraction mapping constant of the system operator in order to

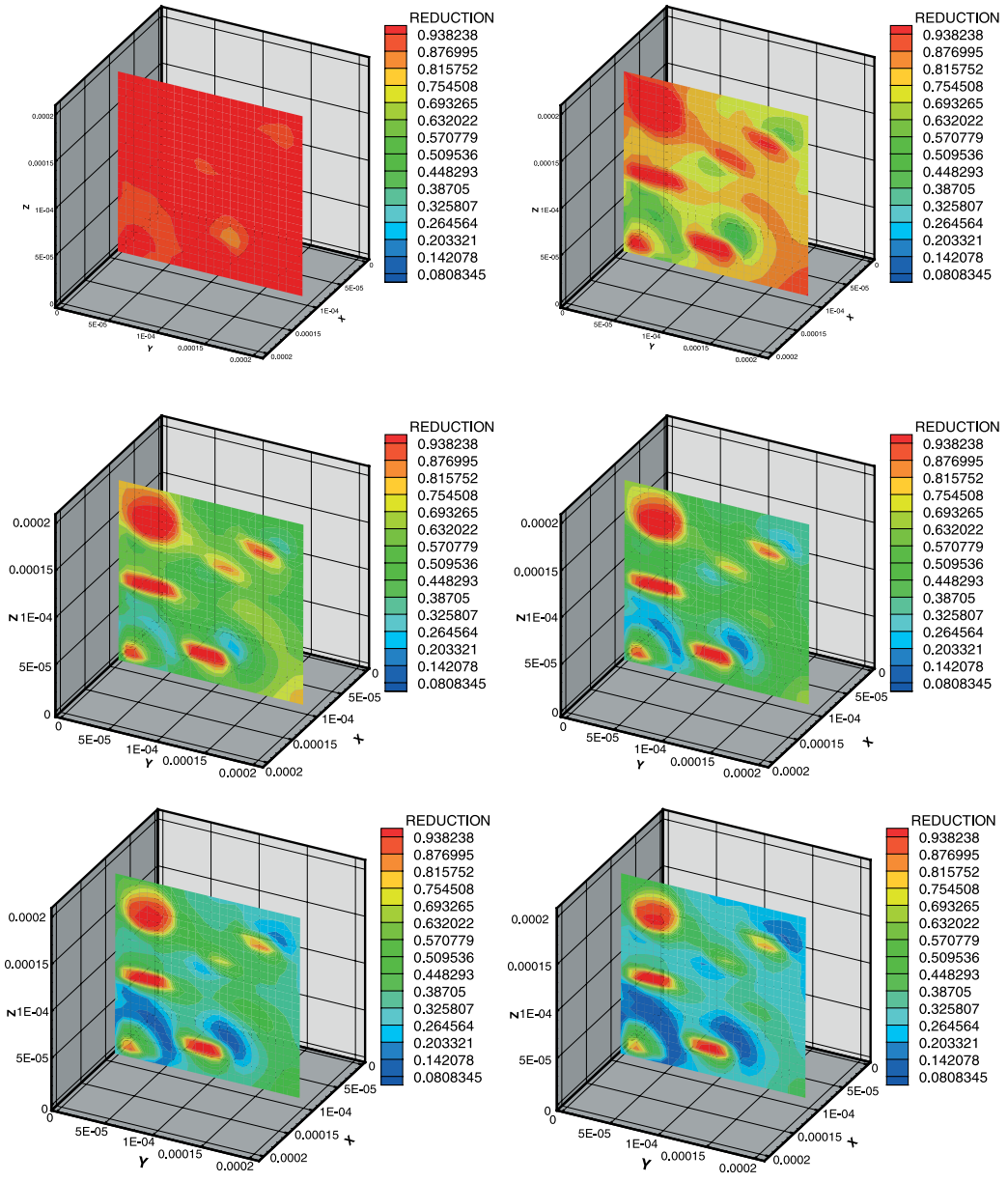

Fig. 9. Starting from the top, left to right: The time history of the degradation (α) throughout the solid, in increments of 0.1 years.

induce desired staggering rates of convergence within each time step. The overall goal was to deliver accurate solutions where the staggering error was controlled while simultaneously obeying time-step size limits dictated by discretization error concerns.

Generally speaking, the staggering error, which is a function of the time step size, is temporally variable and can become stronger, weaker, or possibly oscillatory, is extremely difficult to ascertain a-priori as a function of the time step size. Therefore, to circumvent this problem, the adaptive strategy presented in this

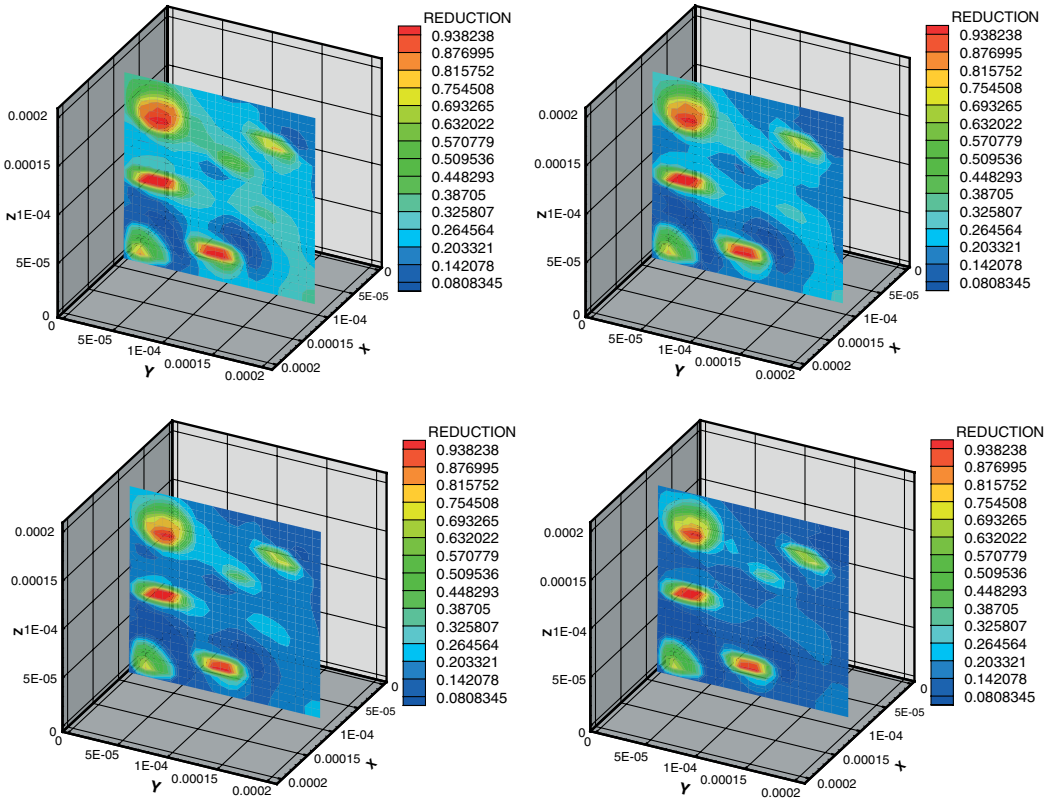

Fig. 10. Starting from the top, left to right: The time history, continued from Fig. 9, of the degradation (α) throughout the solid, in increments of 0.1 years.

work was developed to provide accurate solutions by iteratively adjusting the time steps. Specifically, a sufficient condition for the convergence of the presented fixed-point scheme was that the spectral radius or contraction constant of the coupled operator, which depends on the time step size, must be less than unity. This observation was used to adaptively maximize the time step sizes, while simultaneously controlling the coupled operator's spectral radius, in order to deliver solutions below an error tolerance within a pre-specified number of desired iterations. This recursive staggering error control can allow for substantial reduction of computational effort by the adaptive use of large time steps. Furthermore, such a recursive process has a reduced sensitivity, relative to an explicit staggering approach, to the order in which the individual equations are solved, since it is self-correcting.

In the ideal case, one would like to make predictions of whether a certain type of matrix-particulate combination will have poor multifield and inelastic behavior via numerical simulations, in order to minimize expensive laboratory tests. As an extension to this work, emphasis should be placed on microstructural optimization to resist severe-loading environments. For example, this could involve the construction of an inverse problem, where combinations of particulate and matrix materials are sought to minimize the following history-dependent objective function:

$$\Pi = \int_0^{\mathrm{T}} \left(\frac{\| \langle \boldsymbol{\sigma}(\boldsymbol{x},t) \rangle_{\Omega} - \boldsymbol{\sigma}^D(t) \|}{\| \boldsymbol{\sigma}^D(t) \|} \right) \mathrm{d}t + \text{Constraints}, \tag{6.1}$$

where $\boldsymbol{\sigma}(\boldsymbol{x}, t)$ is the microscopic stress response of the material, $\boldsymbol{\sigma}^D(t)$ is a prespecified desired effective macroscopic stress response, T is the total time interval of interest, and where $\|\cdot\|$ is an appropriate norm. Such an objective function depends in a non-convex and non-differentiable manner on the design parameters. One approach is to employ algorithms which combine gradient methods for local searches with genetic algorithms for global searches. A recent overview of the state of the art of genetic algorithms can be found in a collection of articles edited by Goldberg and Deb [12]. There are a variety of such methods, which employ concepts of species evolution, such as reproduction, mutation and crossover. The application of such ideas to non-multifield material design can be found in Zohdi [65,66].

References

[1] M. Amieur, S. Hazanov, C. Huet, Numerical and experimental study of size and boundary conditions effects on the apparent properties of specimens not having the representative volume, in: C. Huet (Ed.), Micromechanics of Concrete and Cementitious Composite, 1993.

[2] M. Amieur, 1994. Etude numérique et expérimentale des effets d'échelle et de conditions aux limites sur des éprouvettes de béton n'ayant pas le volume représentatif, Doctoral Dissertation No. 1256, Ecole Polytechnique Fédérale de Lausanne, Lausanne, Switzerland.

[3] M. Amieur, S. Hazanov, C. Huet, Numerical and experimental assessment of the size and boundary conditions effects for the overall properties of granular composite bodies smaller than the representative volume, in: D.F. Parker, A.H. England (Eds.), UTAM Symposium on Anisotropy, Inhomogeneity and Nonlinearity in Solid Mechanics, Kluwer Academic Publishers, The Netherlands, 1995, pp. 149–154.

[4] W.F. Ames, Numerical Methods for Partial Differential Equations, second ed., Academic Press, New York, 1977.

[5] M.A. Ashby, D.R.H. Jones, Engineering Materials 2. An Introduction to Microstructures, Processing and Design, Pergamon Press, 1992.

[6] O. Axelsson, Iterative Solution Methods, Cambridge University Press, Cambridge, 1994.

[7] J. Crank, The Mathematics of Diffusion, second ed., Oxford Science Publications, Oxford, 1975.

[8] I.St. Doltsinis, Coupled field problems—solution techniques for sequential and parallel processing, in: M . Papadrakakis (Ed.), Solving large-scale problems in mechanics, 1993.

[9] I.St. Doltsinis, Solution of coupled systems by distinct operators, Eng. Comput. 14 (1997) 829–868.

[10] C.P. Flynn, Point Defects and Diffusion, Clarendon Press, Oxford, 1972.

[11] S.P. Frankel, Convergence rates of iterative treatments of partial differential equations, Math. Tables Aids Comput. 4 (1950) 65–75.

[12] D.E. Goldberg, K. Deb, Special issue on genetic algorithms, Comput. Methods Appl. Mech. Eng. 186 (2–4) (2000) 121–124.

[13] A. Guidoum, P. Navi, Numerical simulation of thermo-mechanical behaviour of concrete through a 3-D granular cohesive model, in: C. Huet (Ed.), Micromechanics of Concrete and Cementitious Composites, Presses Polytechniques et Universitaires Romandes, Lausanne, 1993, pp. 213–228.

[14] A. Guidoum, Simulation numèrique 3D des comportements des bètons en tant que composites granulaires, Doctoral Dissertation No. 1310, Ecole Polytechnique de Lausanne, Switzerland, 1994.

[15] S. Hazanov, C. Huet, Order relationships for boundary conditions effect in heterogeneous bodies smaller than the representative volume, J. Mech. Phys. Solids 42 (1994) 1995–2011.

[16] S. Hazanov, M. Amieur, On overall properties of elastic heterogeneous bodies smaller than the representative volume, Int. J. Eng. Sci. 33 (9) (1995) 1289–1301.

[17] C. Huet, Thermo-hygro-mechanical couplings in wood technology and rheological behaviours, in: H.D. Bui, Q.S. Nguyen (Eds.), Thermomechanical Couplings in Solids, IUTAM Symposium, Paris, 1986, North-Holland, 1987, pp. 163–182.

[18] C. Huet, Modelizing the kinetics of the thermo-hygro-viscoelastic behavior of wood under constant climatic conditions, in: R. Itani (Ed.), Proceedings of the 1988 International Conference on Timber Engineering, Seattle, 1988, pp. 395–401.

[19] C. Huet, Hybrid continuum thermodynamics framework and numerical simulations examples for the delayed micromechanical behavior of heterogeneous materials with chemical, climatic and defect sensitivity, in: Q.S. Nguyen, V.D. Nguyen (Eds.), Engineering Mechanics Today, Proc. Int. Conf. Hanoi, University of Hanoi, 1995, pp. 170–184.

[20] C. Huet, A. Guidoum, P. Navi, A 3D micromechanical model for numerical analysis and prediction of long term deterioration in concrete, in: K. Sakai, N. Banthia, O.E. Gjorv (Eds.), Concrete Under Severe Conditions: Environment and Loading, Vol. 2, Spon, London, 1995, pp. 1458–1467.

[21] C. Huet, Recent advances in the long term deformation and deterioration behavior of structural materials and components through the integrated micromechanics and thermodynamics of solids approach, in: A. Gerdes (Ed.), Advances in Building Materials, Aedificatio, Freiburg, 1996, pp. 161–196.

[22] C. Huet, Activities 1989–1996, in: P. Navi, A. Tolou (Eds.), Laboratory for Building Materials, Department of Materials Report, 1997.
[23] C. Huet, An integrated micromechanics and statistical continuum thermodynamics approach for studying the fracture behaviour of microcracked heterogeneous materials with delayed response, Eng. Fract. Mech. 58 (5–6) (1997) 459–556.
[24] C. Huet, Coupled size and boundary condition effects in viscoelastic heterogeneous bodies, Mech. Mater. 31 (12) (1999) 787–829.
[25] C. Huet, Remarques sur l'assimilation d'un matériau hétérogéne á un milieu continu équivalent, in: C. Huet, A. Zaoui (Eds.), Rheological behaviour and Structure of Materials, Presses ENPC, Paris, 1981, pp. 231–245.
[26] C. Huet, Universal conditions for assimilation of a heterogeneous material to an effective medium, Mech. Res. Commun. 9 (3) (1982) 165–170.
[27] C. Huet, On the definition and experimental determination of effective constitutive equations for heterogeneous materials, Mech. Res. Commun. 11 (3) (1984) 195–200.
[28] C. Huet, Application of variational concepts to size effects in elastic heterogeneous bodies, J. Mech. Phys. Solids 38 (1990) 813–841.
[29] C. Huet, Hierarchies and bounds for size effects in heterogeneous bodies, in: G.A. Maugin (Ed.), Continuum Models and Discrete Systems, Vol. 2, 1991, pp. 127–134.
[30] C. Huet, P. Navi, P.E. Roelfstra, A homogenization technique based on Hill's modification theorem, in: Continuum Models and Discrete Systems, 1991.
[31] L.M. Kachanov, Introduction to Continuum Damage Mechanics, Martinus Nijoff, Dordrecht, 1986.
[32] J. Kitchen, Concerning the convergence of iterates to fixed points, Studia Math. 27 (1966) 247–249.
[33] X. Markenscoff, Diffusion induced instability, Quart. Appl. Mech. LIX (1) (2001) 147–151.
[34] X. Markenscoff, Instabilities of a thermo-mechano-chemical system, Quart. Appl. Mech. LIX (3) (2001) 471–477.
[35] X. Markenscoff, On conditions of "negative creep" in amorphous solids, Mech. Mater. 35 (3–6) (2003) 553–557.
[36] M.A. Meyers, L.H. Yu, K.S. Vecchio, Shock synthesis in silicides-II. Thermodynamics and kinetics, Acta Metall. Mater. 42 (3) (1994) 715–729.
[37] M.A. Meyers, Dynamic Behavior of Materials, John-Wiley, New York, 1994.
[38] P. Le Tallec, J. Mouro, Fluid structure interaction with large structural displacements, Comput. Methods Appl. Mech. Eng. 190 (24–25) (2001) 3039–3067.
[39] R.W. Lewis, B.A. Schrefler, The Finite Element Method in the Static and Dynamic Deformation and Consolidation of Porous Media, second ed., Wiley Press, New York, 1998.
[40] R.W. Lewis, B.A. Schrefler, L. Simoni, Coupling versus uncoupling in soil consolidation, Int. J. Num. Anal. Metho. Geomech. 15 (1992) 533–548.
[41] S. Nemat-Nasser, M. Hori, Micromechanics: Overall Properties of Heterogeneous Solids, second ed., Elsevier, Amsterdam, 1999.
[42] V.F. Nesterenko, Dynamics of Heterogeneous Materials, Springer-Verlag, Berlin, 2001.
[43] V.F. Nesterenko, M.A. Meyers, H.C. Chen, J.C. LaSalvia, Controlled high rate localized shear in porous reactive media, Appl. Phys. Lett. 65 (24) (1994) 3069–3071.
[44] J. Ortega, M. Rockoff, Nonlinear difference equations and Gauss–Seidel type iterative methods, SIAM J. Numer. Anal. 3 (1966) 497–513.
[45] A. Ostrowski, Les points d' attraction et de r'epulsion pour l'it'eration dans l'espace a' n dimensions, C.R. Acad. Sci. Paris 244 (1957) 288–289.
[46] A. Ostrowski, Solution of Equations and Systems of Equations, Academic Press, New York, 1966.
[47] K.C. Park, C.A. Felippa, Partitioned analysis of coupled systems, in: T. Belytschko, T.J.R. Hughes (Eds.), Computational Methods for Transient Analysis, 1983.
[48] O. Perron, Über Stabilität und asymptotisches Verhalten der Lösungen eines Systems endlicher Differenzengleichungen, J. Reine Angew. Math. 161 (1929) 41–64.
[49] S. Piperno, Explicit/implicit fluid/structure staggered procedures with a structural predictor and fluid subcycling for 2D inviscid aeroelastic simulations, Int. J. Num. Meth. Fluids. 25 (1997) 1207–1226.
[50] L. Schmidt, The Engineering of Chemical Reactions, Oxford University Press, Oxford, 1998.
[51] B.A. Schrefler, A partitioned solution procedure for geothermal reservoir analysis, Comm. Appl. Num. Meth. 1 (1985) 53–56.
[52] J. Shackelford, Introduction to Materials Science for Engineers, fourth ed., Macmillan Publishers, 1996.
[53] R.V. Southwell, Relaxation Methods in Engineering Science, Oxford University Press, New York, 1940.
[54] R.V. Southwell, Relaxation Methods in Theoretical Physics, Oxford University Press, New York, 1946.
[55] N.N. Thadhani, Shock-induced chemical reactions and synthesis of materials, Progr. Mater. Sci. 37 (1993) 117–226.
[56] K.S. Vecchio, M.A. Meyers, Shock synthesis in silicides-I. Experimentation and microstructural evolution, Acta Metall. Mater. 42 (3) (1994) 701–714.
[57] D.M. Young, Iterative methods for solving partial difference equations of elliptic type. Doctoral Thesis, Harvard University, 1950.
[58] O.C. Zienkiewicz, Coupled problems and their numerical solution, in: R.W. Lewis, P. Bettes, E. Hinton (Eds.), Numerical Methods in Coupled Systems, Wiley, Chichester, 1984, pp. 35–58.

[59] T.I. Zohdi, An adaptive-recursive staggering strategy for simulating multifield coupled processes in microheterogeneous solids, Int. J. Numer. Methods Eng. 53 (2002) 1511–1532.
[60] T.I. Zohdi, Staggering error control for a class of inelastic processes in random microheterogeneous solids, Int. J. Nonlinear Mech. (39) (2004) 281–297.
[61] T.I. Zohdi, Some remarks on hydrogen trapping, Int. J. Fract. 106 (2) (2000) L9–L14.
[62] T.I. Zohdi, Simulation of time-discontinuous chemically aided intergranular fracture, Comput. Mater. Sci. 24 (4) (2002) 490–500.
[63] T.I. Zohdi, Computational optimization of vortex manufacturing of advanced materials, Comput. Methods Appl. Mech. Eng. 190 (46–47) (2001) 6231–6256.
[64] T.I. Zohdi, P. Wriggers, C. Huet, A method of substructuring large-scale computational micromechanical problems, Comput. Methods Appl. Mech. Eng. 190 (43–44) (2001) 5639–5656.
[65] T.I. Zohdi, Constrained inverse formulations in random material design, Comput. Methods Appl. Mech. Engrg. 192 (28–30) (2003) 3179–3194.
[66] T.I. Zohdi, Genetic optimization of statistically uncertain microheterogeneous solids, Philos. Trans. Roy. Soc.: Math., Phys. Eng. Sci. 361 (1806) (2003) 1021–1043.